The Astronomical Journal, 140:919–924, 2010 October doi:10.1088/0004-6256/140/4/919

HIGH-RESOLUTION 1.6 μm SPECTRA OF FeH IN M AND L DWARFS*,†

Robert J. Hargreaves[1], Kenneth H. Hinkle[2], Charles W. Bauschlicher, Jr.[3], Sebastian Wende[4], Andreas Seifahrt[5], and Peter F. Bernath[1]
[1] Department of Chemistry, University of York, Heslington, York, YO10 5DD, UK; rjh135@york.ac.uk, pfb500@york.ac.uk
[2] National Optical Astronomy Observatory,[6] P.O. Box 26732, Tucson, AZ 85726, USA; hinkle@noao.edu
[3] NASA Ames Research Centre, Mailstop 230-3, Moffett Field, CA 94035, USA; Charles.W.Bauschlicher@nasa.gov
[4] Institut für Astrophysik, Georg-August-Universität Göttingen, Friedrich-Hund-Platz 1, 37077 Göttingen, Germany; sewende@astro.physik.uni-goettingen.de
[5] Department of Physics, University of California, One Shields Avenue, Davis, CA 95616, USA; seifahrt@physics.ucdavis.edu
Received 2010 May 19; accepted 2010 July 19; published 2010 August 17

ABSTRACT

Near-infrared bands due to the iron monohydride (FeH) molecule are a characteristic feature of late-M and -L dwarfs. We have created a line list at 2200 K for the FeH $E\,^4\Pi$–$A\,^4\Pi$ electronic transition near 1.58 μm (6300 cm^{-1}) based on laboratory spectra and an ab initio calculation of the band strength. A variety of M and L dwarfs were observed near 1.6 μm with high spectral resolution ($R \sim 70{,}000$) using the Phoenix spectrograph on the 8.1 m Gemini South telescope. The FeH E–A transition made a surprisingly strong contribution to the observed spectral energy distributions and needs to be included in modeling of late-M and L dwarfs.

Key words: brown dwarfs – infrared: stars – stars: individual (DENIS 1048-39, GJ 191, GJ 406, GJ 644C, LHS 292, LHS 2065, LHS 3003, LP 944-20, 2MASS J1507-16) – stars: low-mass

Online-only material: machine-readable and VO tables

1. INTRODUCTION

The Wing–Ford band is present in the near-infrared spectra of late-M-type stars near 990 nm (Wing & Ford 1969). The molecule responsible for this distinctive feature remained elusive until Nordh et al. (1977) were able to correlate the Wing–Ford band with a band of iron monohydride (FeH) at 989.6 nm. Wing et al. (1977) were also able to identify this band at higher spectral resolution in sunspots. Phillips et al. (1987) carried out the definitive rotational analysis of several bands and proved that the Wing–Ford band was the 0–0 vibrational band of the $F\,^4\Delta_i$–$X\,^4\Delta_i$ electronic transition of FeH.

The spectral energy distributions (SEDs) of late-M-type stars and L dwarfs display absorption bands of many molecular species including the metal hydrides CaH, CrH, and FeH (Kirkpatrick 2005; Bochanski et al. 2007). A strong Wing–Ford band is a characteristic feature of L-type objects (Kirkpatrick 2005). M-type stars (with surface temperatures around 2300–3900 K) have strong oxide bands due to TiO and VO, but as the temperature decreases to that of L-type objects (∼1300–2500 K) the TiO and VO bands become fainter and are replaced by CrH and FeH bands (Kirkpatrick et al. 1999). The bands from these molecules remain distinguishing features until the temperature reaches that of T-type brown dwarfs (∼800–1300 K) and then CrH and FeH fade, vibration-rotation bands of H_2O strengthen, and CH_4 appears (Burgasser et al. 2006).

Wallace & Hinkle (2001b) identified 68 lines of a new infrared band system of FeH at 1.58 μm (6300 cm^{-1}) in the spectrum of a cool sunspot (Wallace & Hinkle 2001a) by comparison with a laboratory spectrum. On the basis of ab initio calculations of the properties of the low-lying electronic states by Langhoff & Bauschlicher (1990), the lines were tentatively assigned to the 0–0 vibrational band of the $E\,^4\Pi_i$–$A\,^4\Pi_i$ electronic transition. Some of these FeH lines were also seen weakly in the spectrum of the early-M star GJ 411 (M2+ V) and more strongly in the late-M star GJ 569B (M8.5 V). Cushing et al. (2003) used medium-resolution spectra to show that the FeH absorption features near 1.6 μm are prominent in late-M and -L dwarfs (M8 to L7.5). The 0–0 band of $E\,^4\Pi$–$A\,^4\Pi$ FeH transition was rotationally analyzed by Balfour et al. (2004), who noticed an additional infrared electronic transition at 1.35 μm (7400 cm^{-1}) due to the $E\,^4\Pi$–$X\,^4\Delta$ transition.

The lines of the Wing–Ford band and $E\,^4\Pi$–$A\,^4\Pi$ transition show a substantial Zeeman effect in the sunspot spectrum (Wallace & Hinkle 2001b). Magnetically sensitive lines of these transitions are potentially useful in the determination of magnetic fields in M and L objects because suitable atomic lines become difficult to find in cool sources (Reiners & Basri 2006). The molecular g values needed are now available for a number of lines in the $F\,^4\Delta_i$–$X\,^4\Delta_i$ transition based on laboratory Zeeman experiments and the analysis of sunspot data (Harrison et al. 2008a; Harrison & Brown 2008b). As the suitability of a line for magnetic field determinations increases with wavelength, the E–A lines are also potentially useful if g-values can be determined.

Dulick et al. (2003) provided a line list for the $F\,^4\Delta_i$–$X\,^4\Delta_i$ transition based on term values derived from the analysis of Phillips et al. (1987) and extrapolated them to higher v's and J's. Line intensities were based on an ab initio calculation of the transition dipole moment and calculated Hönl–London rotational line strength factors. They were also able to compute molecular opacities for a range of temperatures and pressures encountered in M and L dwarf atmospheres, and the comparison of a calculated SED with an

* Based on observations (GS-2007A-C-2) obtained at the Gemini Observatory, which is operated by the Association of Universities for Research in Astronomy, Inc., under a cooperative agreement with the NSF on behalf of the Gemini partnership: the National Science Foundation (USA), the Science and Technology Facilities Council (UK), the National Research Council (Canada), CONICYT (Chile), the Australian Research Council (Australia), Ministério da Ciência e Tecnologia (Brazil), and Ministerio de Ciencia, Tecnología e Innovación Productiva (Argentina).
† Based on observations obtained with the Phoenix infrared spectrograph, developed and operated by the National Optical Astronomy Observatory.
[6] Operated by Association of Universities for Research in Astronomy, Inc., under cooperative agreement with the National Science Foundation.

Table 1
Observational Log of Objects

Source	Spectral Type	Magnitude (K)	Total Integration (minutes)
GJ 191	M6	5.1	4
LHS 292	M6	8.0	20
GJ 406	M6	6.1	1
LHS 3003	M6	8.9	20
GJ 644C	M7	8.8	20
LP 944-20	M9	9.5	80
LHS 2065	M9	10.0	80
DENIS 1048-39	M9	8.6	20
2MASS J1507-16	L5	11.3	60

Note. The reduced program star spectra are shown in Figure 2.

observed L5 dwarf spectrum showed reasonable agreement at low resolution.

In this paper, we report on our line list for the FeH $E\,^4\Pi$–$A\,^4\Pi$ transition near 1.58 μm (6300 cm^{-1}) based on a combination of laboratory spectra and ab initio calculations, and our high-resolution observations of a series of M and L dwarfs.

2. ASTRONOMICAL OBSERVATIONS

High-resolution infrared spectra were obtained for target M and L dwarfs using the 8.1 m Gemini South reflecting telescope and the NOAO Phoenix spectrometer (Hinkle et al. 1998). The observations (GS-2007A-C-2) were carried out during one night, 2007 March 2. The program stars, listed in Table 1, were selected to be bright representatives of their spectral subclass. The sample brackets the mid-M to mid-L spectral types. In addition, hot stars with no intrinsic spectral lines in the regions observed were observed to remove fringing and telluric lines. A set of ten flats and darks was also observed.

The Phoenix spectrometer is a cryogenically cooled echelle spectrograph that uses order-separating filters to isolate individual echelle orders. The detector is a 1024×1024 InSb Aladdin II array. The size of the detector in the dispersion direction limits the wavelength coverage in a single observation to about 0.5% (1550 km s^{-1}, or ~80 Å at 1.6 μm). One edge of the detector is blemished, so the wavelength coverage on all but the brightest sources is typically trimmed by a few percent to avoid this area. The spectra discussed here were observed with the two pixel slit resulting in a spectral resolving power of $R = \lambda/\Delta\lambda \sim 70{,}000$. The two pixel wide slit is narrow on the sky, 0.″18, so there were significant slit losses. However, the highest possible resolution was felt to be appropriate for this program. The spectral region observed was centered on 1.6524 μm = 6050 cm^{-1}.

Each program star was observed at two different positions along the slit separated by 6″ on the sky. While seeing varied during the observations, the typical delivered image quality was subarcsecond so stellar images at different positions on the slit were well separated on the detector. Each observation was ratioed to an average flat minus an average dark. Differencing the observations at two different positions along the slit then removed sky and dark backgrounds. The array image frames were then reduced to one-dimensional spectra using the IRAF routine APALL.

The wavelength calibrations were computed by using a set of telluric wavelengths obtained from the hot-star spectra. A number of telluric lines, mostly fairly weak, are present in the spectral interval observed. Using the IRAF routine TELLURIC, the program stars were ratioed to the hot-star spectra. This worked well to remove the telluric spectrum and to remove any fringing present. In practice, virtually no evidence of telluric absorption is visible in the program star spectra.

Table 2
Summary of the MRCI+Q Results

State	r_e (Å)	D_0 (eV)	ω_e (cm^{-1})	$\omega_e x_e$ (cm^{-1})	T_e(cm^{-1})
X	1.564	1.54	1777.1	32.3	0
A	1.545	1.58	1799.1	34.3	–408
E	1.645	1.80	1579.1	31.8	7263

3. AB INITIO CALCULATION OF BAND STRENGTH (COMPUTATIONAL APPROACH)

The calculations are very similar to those performed for our study (Dulick et al. 2003) of the FeH F–X transition. In order to obtain an equivalent treatment of the E, A, and X states, we optimize the orbitals using the state-averaged complete-active-space self-consistent-field (SA-CASSCF) approach, with equal weights for each state. The SA-CASSCF calculations are performed using symmetry and equivalence restrictions and therefore the wave functions have $C_{\infty v}$ symmetry even though the calculations are performed in C_{2v} symmetry. The active space consists of the Fe $3d$, $4s$, and $4p$ orbitals and the H $1s$ orbital plus one additional σ orbital based on preliminary calculations. In C_{2v} symmetry, this corresponds to an active space of six a_1, two b_1, two b_2, and one a_2 orbitals. More extensive correlation is included using the internally contracted multireference configuration interaction approach (IC-MRCI; Werner & Knowles 1988; Knowles & Werner 1988). The CASSCF configurations are used as reference configurations in the IC-MRCI calculations and only the valence electrons are correlated. We estimate the effect of higher excitations using the Davidson correction, which is denoted by $+Q$. We obtain one state of A_1 symmetry and three states of B_1 symmetry, because there is a $^4\Phi$ state between the $E\,^4\Pi$ and $A\,^4\Pi$ states for some internuclear separations. It is easy to identify the Φ state as there is little mixing between the Φ and Π states even though the IC-MRCI calculations are performed in C_{2v} symmetry. Scalar relativistic effects are included using the one-electron Douglas–Kroll (DK) approach (Hess 1986).

The Fe basis set can be described as $(20s15p10d6f4g)/[7s7p5d3f2g]$. The primitive set is derived from that of Partridge (1989). The s, p, and d primitives are contracted based on a DK-SCF calculation of the ^5D state of the Fe atom. The inner 16 s primitives are contracted to three functions and the outermost four are uncontracted, the inner ten p primitives are contracted to two functions and the outermost five are uncontracted, and the inner six d primitives are contracted to one function and the outermost four are uncontracted. The f and g sets are taken from our averaged atomic natural orbital set (Bauschlicher 1995). For hydrogen, the correlation-consistent polarized-valence triple zeta set (Dunning 1989) is used, but the contraction coefficients are taken from a DK-SCF calculation. The CASSCF/IC-MRCI calculations are performed using Molpro (Werner & Knowles 2002). The computational results are summarized in Table 2 for the equilibrium bond length, r_e; the dissociation energy from $v = 0$, D_0; the equilibrium vibrational frequency, ω_e; the vibrational anharmonic correction, $\omega_e x_e$; the term energy measured from equilibrium, T_e. Table 3 provides the Einstein $A_{v'v''}$ values for the $v' - v''$ vibrational bands.

Table 3
Einstein Coefficients

	$A_{v'v''}$	E (cm^{-1})	A (s^{-1})	$A_{v'v''}$	E (cm^{-1})	A (s^{-1})
E–A	A_{00}	7230.2	0.1312(+5)	A_{22}	6855.3	0.1062(+5)
	A_{01}	5526.0	0.1038(+3)	A_{23}	5293.5	0.2830(+3)
	A_{02}	3891.0	0.1557(+0)	A_{24}	3810.0	0.6775(+0)
	A_{10}	8745.0	0.4096(+1)	A_{30}	11577.5	0.2719(+2)
	A_{11}	7041.0	0.1188(+5)	A_{31}	9873.4	0.1931(+3)
	A_{12}	5405.8	0.1988(+3)	A_{32}	8238.4	0.1626(+3)
	A_{13}	3844.1	0.4569(+0)	A_{33}	6676.6	0.9332(+4)
	A_{20}	10194.4	0.9456(+2)	A_{34}	5193.1	0.3479(+3)
	A_{21}	8490.3	0.4743(+2)	A_{35}	3794.5	0.4631(+0)
E–X	A_{00}	6160.7	0.1458(+6)	A_{22}	5739.8	0.3051(+5)
	A_{01}	4431.6	0.1481(+5)	A_{23}	4160.5	0.2380(+5)
	A_{02}	2775.5	0.1898(+3)	A_{24}	2662.7	0.7353(+3)
	A_{10}	7675.5	0.6539(+5)	A_{30}	10508.0	0.5906(+4)
	A_{11}	5946.4	0.7093(+5)	A_{31}	8779.0	0.4110(+5)
	A_{12}	4290.3	0.2166(+5)	A_{32}	7122.9	0.6905(+5)
	A_{13}	2711.1	0.4576(+3)	A_{33}	5543.7	0.1073(+5)
	A_{20}	9124.9	0.2088(+5)	A_{34}	4045.8	0.2341(+5)
	A_{21}	7395.9	0.7925(+5)	A_{35}	2635.6	0.9737(+3)

Table 4
Parameters Used for the PGOPHER Simulation of the $E\,^4\Pi$–$A\,^4\Pi$ Transition of FeH

Temperature (K)		2200	[a]
S_{00} (D^2)		1.391	[b]
$E\,^4\Pi$	Energy	7416	[c]
	A	−145	[d]
	B	6.39098	[d]
	D	4.30×10^{-4}	[d]
$A\,^4\Pi$	Energy	1200	[c]
	A	−120	[d]
	B	7.2830	[d]
	D	5.9×10^{-4}	[d]

Notes. Units are in cm^{-1} unless otherwise stated.
[a] Estimated from relative line intensities in the NSO laboratory spectrum of FeH.
[b] Obtained from the ab initio calculation of the band strength.
[c] Values taken from Langhoff & Bauschlicher (1990).
[d] Values taken from Balfour et al. (2004).

4. LINE STRENGTHS AND LINE LISTS

The line list was generated by determining the intensities of all the peaks contained in the $E\,^4\Pi$–$A\,^4\Pi$ region (4990–6320 cm^{-1}) of the FeH archived spectrum (1983/01/19#2) from the National Solar Observatory (NSO). The FeH spectrum was recorded in 1983 with the Fourier transform spectrometer of the McMath-Pierce Solar Telescope using InSb detectors at a resolution of 0.05 cm^{-1}. It contains thermal emission from a King-type carbon tube furnace loaded with iron filings and a mixed atmosphere of hydrogen and helium operating at 2400°C and ∼250 Torr (experimental details are taken from the log sheet). Phillips et al. (1987) used spectra taken at the same time and explain in more detail the experimental setup.

The lines in the NSO spectrum were measured using WSpectra (Carleer 2001) to generate a line list containing the wavenumber and intensity of 6357 lines. The region studied (4990–6320 cm^{-1}) contains lines primarily from the $E\,^4\Pi_i$–$A\,^4\Pi_i$ electronic transition, and includes numerous unidentified lines. From this list, 262 lines (including Q-branches) were successfully assigned using term values taken from Balfour et al. (2004). For these identified lines, we have also included in the line list the calculated Einstein A value, lower state J value, branch, Ω value, lower state energy, and lower state e/f parity. The lower state energy values for all unidentified lines (96% of all lines) are estimated as the average of all the lower state values from the identified lines (i.e., 2250 cm^{-1}).

The intensity values quoted in the line list are actually line strengths (S') in HITRAN units (cm molecule^{-1}). In SI units, S' is defined (Bernath 2005) as

$$S' = \frac{2\pi\nu_{10}S_{J'J''}}{3\varepsilon_0 hcQ}\exp\left(-\frac{E_0}{kT}\right)\left[1-\exp\left(-\frac{h\nu_{10}}{kT}\right)\right]. \quad (1)$$

The factor $S_{J'J''}$ is the square of the transition dipole moment and Q is the internal partition function. S' values are line intensities as used in the HITRAN database of molecular line parameters (Rothman et al. 2009). Using S', the Beer–Lambert law for the transmission, τ, of radiation through a path length l is given by

$$\tau = \frac{I}{I_0} = \exp[-S'g(\nu-\nu_{10})Nl] \quad (2)$$

in which $g(\nu-\nu_{10})$ is a normalized line shape function and N is the total concentration (and applies only at a certain temperature, T).

The NSO laboratory emission spectrum of FeH was fitted with Voigt lineshape functions using the WSpectra program which provides line positions (cm^{-1}) and line intensities (arbitrary units). There was no need to calibrate the wavenumber scale as known CN lines were found to agree satisfactorily (±0.005 cm^{-1}) with previous measurements (Ram et al. 2010). The intensity scale proved more difficult to calibrate and this was carried out by simulating the spectrum using PGOPHER (Western 2007). Table 4 lists the constants that were used to calculate the spectrum with PGOPHER. The transition strength, S_{00} (1.391 D^2) was calculated from our Einstein A value for the 0–0 band of the E–A transition ($A_{00} = 1.458 \times 10^5$ s^{-1}), by using

$$S_{00} = \frac{3\varepsilon_0 hc^3 A_{00}}{16\pi^3\nu^3} = \frac{3.188583\times10^6 A_{00}}{\tilde{\nu}^3} \quad (3)$$

from (Bernath 2005). For this calculation, the estimated band origin $\tilde{\nu}$ was taken to be 6216 cm^{-1} (see Table 4).

The simulated spectrum was not a very good match to the observed spectrum, but we only required estimates for the calculated Einstein $A_{J'-J''}$ values of the observed lines. The calculated Einstein $A_{J'-J''}$ values were corrected with a ν^3 factor for the differences between observed and calculated frequencies.

In order to calibrate the intensity scale of the NSO laboratory spectrum we first had to select only the transitions which were known (i.e., calculated from Balfour et al. 2004). This allowed us to determine the integrated cross-section ($\int\sigma d\nu$) from the $A_{J'-J''}$ value (Bernath 2005), with

$$\int\sigma d\nu = \frac{A_{J'\to J''}c^2}{8\pi\nu^2}\frac{2J'+1}{2J''+1} \quad (4)$$

which was then used to calculate S' for each line

$$S' = \int\sigma d\nu\frac{2J''+1}{Q}\exp\left(-\frac{E_0}{kT}\right)\left[1-\exp\left(-\frac{h\nu}{kT}\right)\right]. \quad (5)$$

The equations stated are given in SI units. In order to allow a conversion of S' from SI units (m^2 s^{-1} molecule^{-1}) into

Table 5
Sample Line List of the $E\,^4\Pi - A\,^4\Pi$ Transition of FeH

Wavenumber (cm^{-1})	Intensity (cm molecule^{-1})	E lower (cm^{-1})	Einstein A (s^{-1})	J lower (cm^{-1})	Branch	Ω & Parity
...	...	...	...	...	...	...
6137.8061523	0.6618295E−18	2250.00				
6137.7275391	0.1444019E−18	2250.00				
6137.5366211	0.1247505E−17	1178.08	0.62512580E+05	0.350E+01	R	1.5f
6137.4711914	0.2174224E−17	3756.22	0.71171470E+05	0.185E+02	R	0.5f
6137.3930664	0.7319333E−19	2250.00				
6137.3613281	0.5026452E−18	2250.00				
6137.2729492	0.3660579E−18	2250.00				
6137.0297852	0.1381187E−17	3247.22	0.72471440E+05	0.175E+02	R	1.5e
6136.9233398	0.6917597E−18	2250.00				
6136.7304688	0.1066923E−17	2250.00				
...	...	...	...	...	...	...

(This table is available in its entirety in machine-readable and Virtual Observatory (VO) forms in the online journal. A portion is shown here for guidance regarding its form and content.)

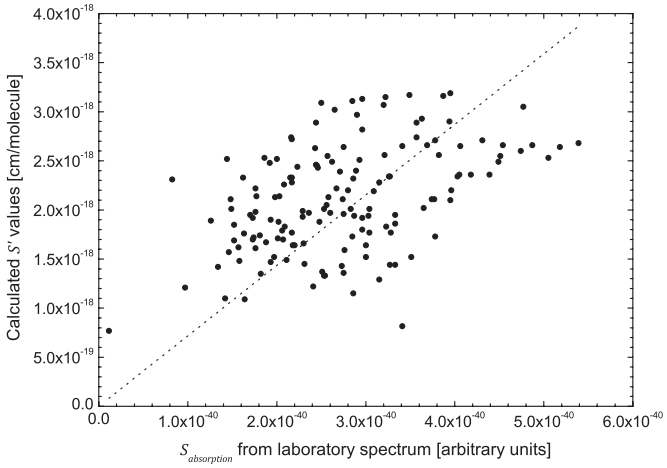

Figure 1. Scatter plot of the calculated line strength values S' and the observed line strength values $S_{\rm absorption}$. The calibration factor of 7.968×10^{21} is shown as the dotted line.

HITRAN units (cm molecule^{-1}) a conversion factor of $100\,c^{-1}$ has to be applied. Pugh & Rao (1976) provide information for converting between various possible units for the line intensity S'.

We were then in a position to transform the laboratory intensities into HITRAN intensities by comparing them to the calculated intensities in HITRAN units. This proved more difficult than it first seemed. After detailed analysis of the laboratory line intensities it was discovered that they more closely resembled emission from FeH at 2200 K (as oppose to 2673 K) and this was the temperature used to calculate the intensities in HITRAN units. The corresponding partition function is given by Dulick et al. (2003) as $Q_{2200\,\rm K} = 5534.78$. The observed intensities ($S_{\rm emission}$) were converted from emission to absorption (Nassar and Bernath 2003) by

$$S_{\rm absorption} = \frac{S_{\rm emission}}{\nu^3 \exp\left(-\frac{h\nu}{kT}\right)}. \quad (6)$$

The linear calibration factor was found to be 7.968×10^{21} (Figure 1). The intensities of all of the lines in the laboratory spectrum of the $E\,^4\Pi$–$A\,^4\Pi$ region were then converted into HITRAN units (at 2200 K) for the final line list.

5. STELLAR MODELS

The spectral line synthesis of the FeH line opacity is done with the line formation computer code SYNTH3 (Kochukhov 2007). With this code, we are able to compute large spectral regions, including all lines in the line list and we account for blends. The pressure broadening was approximated by van de Waals broadening, which becomes important at effective temperatures below 3000 K, and is treated in the hydrogenic approximation (Schweitzer et al. 1996, and references therein). For this we need the ionization energy of FeH which we choose at 6 eV (Wende et al. 2009), although this value differs from the actual value, the effects on the model are negligible. SYNTH3 accounts for H, He, and H_2 as collisional perturbers in the van de Waals broadening. However to match observed line wings of FeH, it is still necessary to apply an enhancement factor as Schweitzer et al. (1996) did for other molecules. An enhancement factor is commonly used for spectral synthesis of molecules and helps to account for collisional perturbations (Wende et al. 2010). We use a factor of 2.5 which has been obtained by comparing model atmospheres to high-resolution spectra.

The underlying atmosphere models are MARCS models (Gustafsson et al. 2008) with solar composition (Grevesse et al. 2007) and in the opacity sampling, all of the available atomic and molecular species were taken into account. We create a sequence of models with effective temperatures of 2500 K, 2700 K, 2900 K, and 3100 K, and $\log g = 5.0$. No dust is included in these calculations, but it would be important at effective temperatures below 2500 K. At these low temperatures, we do not expect any significant influence from convective velocity fields and therefore we include no micro- or macro-turbulent broadening in the line formation (Wende et al. 2009).

6. RESULTS AND DISCUSSION

We have successfully produced a line list for the $E\,^4\Pi_i$–$A\,^4\Pi_i$ region of FeH which can be applied to atmospheric models. The line list contains assigned lines from Balfour et al. (2004) and the remaining lines are unassigned with an estimated average lower state energy of 2250 cm^{-1}. An error of ±5% (±112.5 cm^{-1}) in the estimated lower state energy will result in an error of less than ±0.5% in the calculated intensity for a temperature shift of ±100 K. The assigned lines do not include the $E\,^4\Pi_{-1/2}$–$A\,^4\Pi_{-1/2}$ subband because the lines could not be assigned with

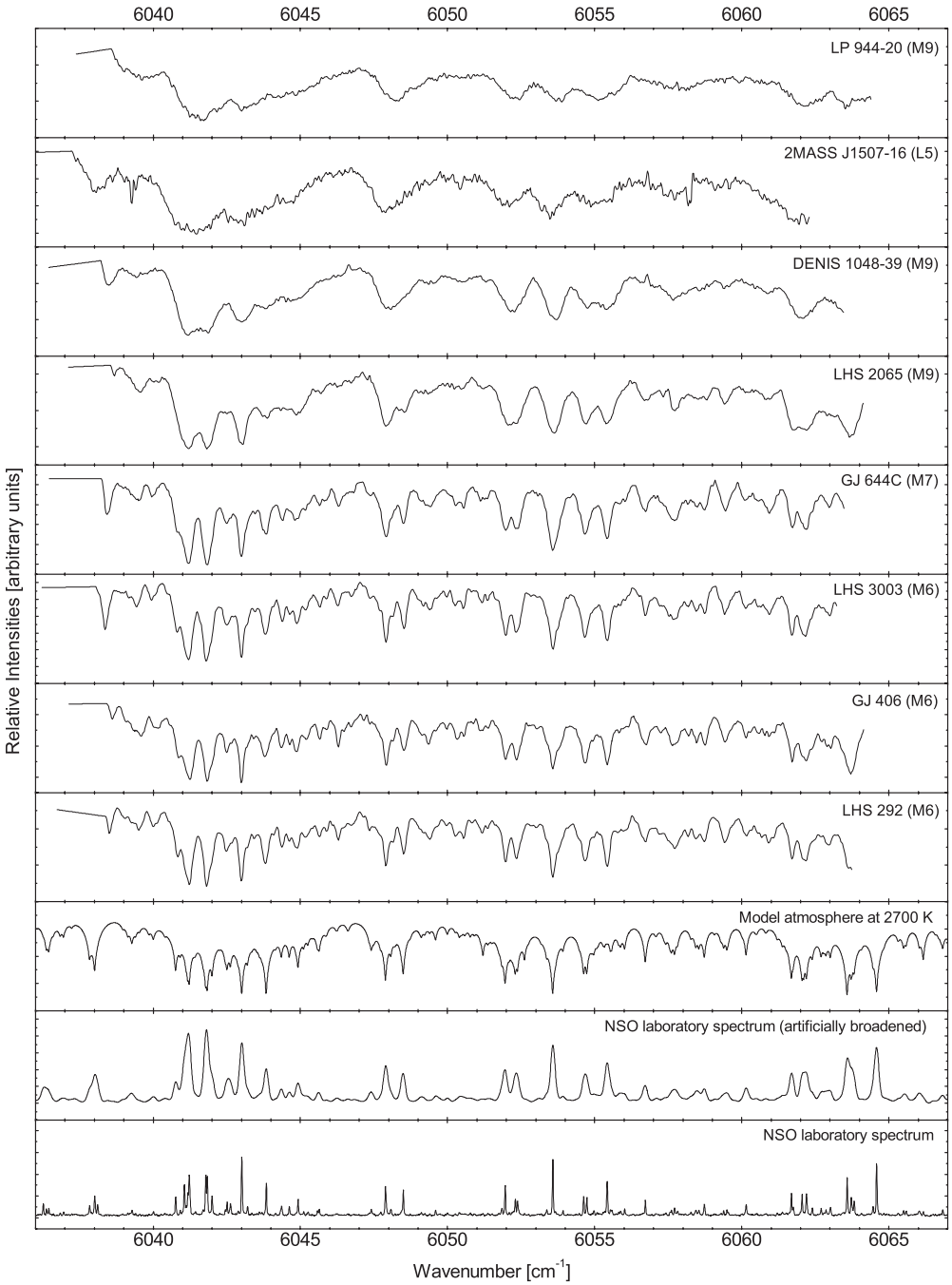

Figure 2. Comparison of the SEDs of observations from the Gemini South observatory with the NSO laboratory spectrum and a model atmosphere containing FeH at 2700 K. Each object has been scaled and plotted on an arbitrary absorption axis.

certainty (Balfour et al. 2004). A sample of the FeH line list is shown in Table 5 and the full line list is available as supplementary material.

Figure 2 shows the observations obtained from the Phoenix spectrograph on Gemini South. What is immediately apparent is the abundance of FeH lines in this region, with almost all of the absorption caused by FeH. Although some of the objects are rapid rotators and the lines suffer from rotational broadening, in particular, LP 944, 2MASS 1507, and DENIS 1048, it is still clear that the FeH absorption lines make a significant contribution to the SED in this region. From these observations, we have been able to successfully identify lines due to the $E\ ^4\Pi$–$A\ ^4\Pi$ transition in the near-infrared spectra of L and M dwarfs. A single setting of the Phoenix spectrograph gave coverage only in the relatively narrow 6036–6064 cm^{-1} region. Although the region is not large, comparison of the observed SEDs with the NSO laboratory spectrum and the 2700 K model we are able to assign almost every feature to the FeH molecule. If we only include the assigned FeH lines into our model, then the spectra are not reproduced, however, inclusion of the unassigned FeH lines gives a very reasonable agreement with the dwarf spectra (see specifically LHS 292 in Figure 2).

The conversion from arbitrary line intensities to HITRAN line intensities as discussed in Figure 1 shows more scatter than expected. The straight line fit is not as good as we would have liked and there are many reasons why this could be the case. We analyzed the laboratory spectrum in detail to try and determine the effective temperature, but we obtained different

values for different Ω components. We settled on a value of 2200 K based on the overall "shape" of the emission. Transition metal hydrides are known to have complicated perturbed spectra and calculations of both line positions and line intensities are unreliable. The E and A states are not isolated and suffer from extensive perturbations which affect both line positions and line intensities. Calculations with programs based on effective Hamiltonians such as PGOPHER do not work well at high-resolution for FeH.

The intensity calibration factor (7.968×10^{21}) was obtained by fitting the points shown in Figure 1. Although the points show considerable scatter, the relative intensities of the lines are based mainly on experimental observations of a sample with a temperature close to that of a late-M or early-L dwarfs. The ab initio calculation of the Einstein A_{00} value is used to provide an absolute intensity calibration. Due to the clear influence of FeH on the SEDs of late-M and -L dwarfs our $E\ ^4\Pi$–$A\ ^4\Pi$ (6320–4990 cm^{-1}) line list should find application in spectral simulations.

7. CONCLUSION

We have obtained a line list at 2200 K for the $E\,^4\Pi_i$–$A\,^4\Pi_i$ FeH transition near 1.6 μm based on experimental measurements and an ab initio calculation of the band strength. The FeH line list can be used in model atmospheres of cool stars and brown dwarfs. The line list contains assigned lines from Balfour et al. (2004) and additional unassigned lines which are included with an estimated average lower state energy (2250 cm^{-1}).

Observations near 1.6 μm were made at high-resolution with the Phoenix spectrograph at Gemini South on L and M dwarfs and almost every feature can be assigned to FeH. When we include the FeH line list in a model atmosphere we are able to match the observed SEDs. We believe that this shows the need to include the $E - A$ FeH line list when modeling late-M and -L dwarfs.

We thank the Gemini South Observatory staff for their technical support during observations. Support for this work was provided by the NASA laboratory astrophysics program and a Department of Chemistry (University of York) studentship. R. J. Hargreaves thanks the Institute of Physics (IOP) and the Department of Physics (University of York) for travel support. A. Seifahrt acknowledges financial support from DFG under grant RE 1664/4-1 and from NSF under grant AST07-08074. S. Wende acknowledges financial support from the DFG Research Training Group GrK-1351 "Extrasolar Planets and Their Host Stars."

Facility: Gemini:South (Phoenix)

REFERENCES

Balfour, W. J., Brown, J. M., & Wallace, L. 2004, J. Chem. Phys., 121, 7735
Bauschlicher, C. W. 1995, Theor. Chim. Acta, 92, 183
Bernath, P. F. 2005, Spectra of Atoms and Molecules (2nd. ed.; Oxford: Oxford Univ. Press)
Bochanski, J. J., West, A. A., Hawley, S. L., & Covey, K. R. 2007, AJ, 133, 531
Burgasser, A. J., Geballe, T. R., Leggett, S. K., Kirkpatrick, J. D., & Golimowski, D. A. 2006, ApJ, 637, 1067
Carleer, M. R. 2001, Proc. SPIE, 4168, 337
Cushing, M. C., Rayner, J. T., Davis, S. P., & Vacca, W. V. 2003, ApJ, 582, 1066
Dulick, M., Bauschlicher, Jr., C. W., Burrows, A., Sharp, C. M., Ram, R. S., & Bernath, P. 2003, ApJ, 594, 651
Dunning, T. H. 1989, J. Chem. Phys., 90, 1007
Grevesse, N., Asplund, M., & Sauval, A. J. 2007, Space Sci. Rev., 130, 105
Gustafsson, B., Edvardsson, B., Eriksson, K., Jørgensen, U. G., Nordlund, Å., & Plez, B. 2008, A&A, 486, 951
Harrison, J. J., & Brown, J. M. 2008, ApJ, 686, 1426
Harrison, J. J., Brown, J. M., Chen, J., Steimle, T. C., & Sears, T. J. 2008, ApJ, 679, 854
Hess, B. A. 1986, Phys. Rev. A., 33, 3742
Hinkle, K. H., Cuberly, R., Gaughan, N., Heynssens, J., Joyce, R., Ridgway, S., Schmitt, P., & Simmons, J. E. 1998, Proc. SPIE, 3354, 810
Kirkpatrick, J. D. 2005, ARA&A, 43, 195
Kirkpatrick, J. D., et al. 1999, ApJ, 519, 802
Knowles, P. J., & Werner, H.-J. 1988, Chem. Phys. Lett., 145, 514
Kochukhov, O. P. 2007, Proc. Int. Conf. Physics of Magnetic Stars, ed. I. I. Romanyuk & D. O. Kudryavtsev, 109
Langhoff, S. R., & Bauschlicher, C. W. 1990, J. Mol. Spectrosc., 141, 243
Nassar, R., & Bernath, P. 2003, J. Quant. Spectrosc. Radiat. Transfer, 82, 279
Nordh, H. L., Lindgren, B., & Wing, R. F. 1977, A&A, 56, 1
Partridge, H. 1989, J. Chem. Phys., 90, 1043
Phillips, J. G., Davis, S. P., Lindgren, B., & Balfour, W. J. 1987, ApJS, 65, 721
Pugh, L. A., & Rao, K. N. 1976, Molecular Spectroscopy: Modern Research, Vol. III (New York: Academic)
Ram, R. S., Wallace, L., & Bernath, P. F. 2010, J. Mol. Spectrosc., in press
Reiners, A., & Basri, G. 2006, AJ, 131, 1806
Rothman, L. S., et al. 2009, J. Quant. Spectrosc. Radiat. Transfer, 110, 533
Schweitzer, A., Hauschildt, P. H., Allard, F., & Basri, G. 1996, MNRAS, 283, 821
Wallace, L., & Hinkle, K. 2001a, NSO Technical Report 01-001 (Tucson, AZ: NSO)
Wallace, L., & Hinkle, K. 2001b, ApJ, 559, 424
Wende, S., Reiners, A., & Ludwig, H.-G. 2009, A&A, 508, 1429
Wende, S., Reiners, A., Seifahrt, A., & Bernath, P. F. 2010, A&A, in press
Werner, H.-J., & Knowles, P. J. 1988, J. Chem. Phys., 89, 5803
Werner, H.-J., & Knowles, P. J. 2002, MOLPRO, Univ. Birmingham (with contributions from Amos R. D. et al.)
Western, C. M. 2007, PGOPHER (v5.2.977), A Program for Simulating Rotational Structure, School of Chemistry, Univ. Bristol (http://pgopher.chm.bris.ac.uk/)
Wing, R. F., Cohen, J., & Brault, J. W. 1977, ApJ, 216, 659
Wing, R. F., & Ford, W. K. 1969, PASP, 81, 527